Preprints of the 21st IFAC World Congress (Virtual)
Berlin, Germany, July 12-17, 2020

Compound robust flight time and heading angle constrained guidance law

Yi Ji*, Pei Pei, Defu Lin*** Jianting Zhao**** and Wei Wang*****

School of Aerospace, Beijing Institute of Technology, Beijing, China, 100081
Beijing Key Laboratory of UAV Autonomous Control, Beijing, China, 100081

** email: yijiinbit@163.com*
***email: 344905714@qq.com*
****email: lindf@bit.edu.cn*
*****email:2220175007@bit.edu.cn*
******email: wangweiyh@bit.edu.cn*

Abstract: This work studies accurate interception problem for salvo-attack missions and proposes a robust guidance law in the presence of impact time and angle constraints. First, the dynamic model for planar homing endgame guidance is built. Different with conventional guidance dynamic model, this work takes the derivative with respect to range, rather than time. Next, the trajectory of desired line-of-sight is formed and a time-to-go prediction method is introduced. On this basis, according to sliding mode methodology, a sliding manifold consisting the knowledge of time-to-go and line-of-sight angle is built and an integrated Lyapunov control method based guidance law is deduced to force this sliding manifold converge to a small region around zero in finite time, so that the missile will intercept target with a desired flight time and a heading angle. Detailed theoretical analysis and numerical simulations verified above properties.

Keywords: homing guidance; salvo attack; flight time constraint; heading angle constraint; sliding mode control.

1. INTRODUCTION

Facing ballistic missile defence system, the so-called "salvo-attack" which requires multiple missiles carry out different flight envelopes and intercept the target simultaneously, is one of the useful methods for defence penetration. Ref.(Yang et al., 2016, He and Lin, 2018, Cho et al., 2015) pointed that this combat method held important significance, especially when it was applied into anti-ship missions to penetrate warships' self-defence system, such as close-in weapon (CIW) and surface-to-air missile (SAM) systems. Obviously, guaranteeing multiple missiles attack the target at the same time is the key-point for salvo-attack.

Generally speaking, there are two methods to achieve salvo-attack: cooperative guidance (Lyu et al., 2019a, Lyu et al., 2019b, Wang and Tan, 2018) and so-called pseudo cooperative guidance (Zhu et al., 2019, Zhao et al., 2016). The key different between these two methods is whether there exists information communication among every interceptor. The former one requires a complex telecommunication system and a cooperative algorithm, which is difficult to apply in real engineering practice. The latter one requires a desired time before missiles launching. Compared with cooperative guidance, this method is much more practical in today's technical environment, although this desired time should be estimated by an experienced engineer. With this in mind, this work concentrates to design a guidance law for so-call pseudo cooperative guidance.

In real engineering practice, zero miss-distance is not the the index to evaluate a guidance law. For single missiles, especially for anti-tank and anti-ship missiles, the impact angle which decides the damage performance in some degree, is another important index. Because of its zero-miss distance property and successful history of application, conventional proportional navigation (PN) guidance law (Talole et al., 2006, Zarchan, 1995, Franzini et al., 2017) is used in many kinds of real engineering missions. However, owing to the limit of field-of-view (FOV), conventional PN guidance law is difficult to be employed in large impact angle attack. With the development of optimal control theory, many scholars aim to design optimal guidance laws with impact angle constraint (Kumar et al., 2014, Bardhan and Ghose, 2015, Tsalik and Shima, 2016) However, these optimal guidance laws are always built on the basis of small attack angle assumption and are difficult to realize large impact angle. Even if these guidance laws take into account the large angles, the complex Hamilton-Jacobi-Bellman equation always does not have an explicit solution.

Because sliding mode control (SMC) method holds strong robustness and can resist the external disturbance, many scholars use it in impact angle constrained guidance law design. To cite a few, Ref.(Hou et al., 2019) proposed two different terminal sliding mode surfaces such that the guidance law can achieve impact time and angle constraints simultaneously; using fast terminal SMC method, Ref.(Sun et al., 2016) presented a guidance law to realize terminal angle

guidance. Ref.(Ji et al., 2019) extend SMC guidance laws into three-dimensional environment.

This work presents an impact time and angle constrained guidance law, which can be applied in salvo-attack missions. The rest of this paper is organized as follows: Sect.2 states problem formulation, consisting with dynamic model, desired line-of-sight (LOS) angle and a time-to-go estimation method; a SMC based guidance law is presented in Sect.3 with a sliding manifold which includes the knowledge of heading angle and flight time. In Sect.4, detailed numerical simulations are carried out to verify the efficiency of proposed guidance law. A brief conclusion is given in Sect.5.

2. PROBLEM FORMULATION

2.1 Dynamic model of engagement phase

Assume that the control system of interceptor holds roll channel stabilization and so that the geometry of endgame engagement phase is built in an inertial Cartesian coordinate $O-XYZ$, as shown as Fig.1.

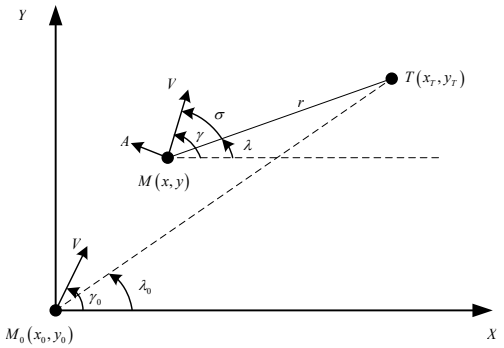

Fig.1 Geometry of endgame engagement phase

In Fig.1, M and T denotes positions of missile and target, (x,y) and (x_T,y_T) denote their coordinates, respectively. $M_0(x_0,y_0)$ denotes initial position of missile, V denotes missile velocity, A denotes missile acceleration and r denotes the distance between the missile and target. γ and λ denote pitch and line-of-sight (LOS) angles, respectively. For ease of study, we denote so-called trajectory lead angle as $\sigma=\gamma-\lambda$.

According to Fig.1, one can conclude the dynamics during engagement phase as

$$\begin{aligned}&\frac{dx}{dt}=V\cos\gamma,\ \frac{dy}{dt}=V\sin\gamma\\&\frac{d\gamma}{dt}=\frac{A}{V},\ \frac{d\lambda}{dt}=-\frac{\sin(\gamma-\lambda)}{r}\\&\frac{dr}{dt}=-V\cos(\gamma-\lambda)\end{aligned}\tag{1}$$

For ease of following calculation, introduce auxiliary variable ζ satisfying

$$\frac{d\zeta}{dx}=\frac{d\zeta}{dt}\frac{dt}{dx}\tag{2}$$

Hence, (1) can be rewritten as

$$\begin{aligned}&t'=\frac{dt}{dx}=\frac{1}{V\cos\lambda},y'=\frac{dy}{dx}=\tan\lambda\\&\gamma'=\frac{d\gamma}{dx}=\frac{A}{V^2\cos\lambda},\lambda'=\frac{d\lambda}{dx}=-\frac{\sin(\gamma-\lambda)}{r\cos\gamma}\\&r'=\frac{dr}{dx}=-\frac{\cos(\gamma-\lambda)}{\cos\gamma}\end{aligned}\tag{3}$$

This completes the dynamics during endgame engagement phase.

Remark 1. Using (2), the time t is released as a system state, which is much easier for following flight time constrained guidance law design.

2.2 Desired LOS angle formulation

According to linear approximation methodology, desired LOS angle and its derivative with respect to x is formulated as

$$\begin{aligned}&\lambda_d(x)=a\frac{x^3}{x_T^3}+b\frac{x^2}{x_T^2}+c\frac{x}{x_T}+d\\&\lambda_d'(x)=3a\frac{x^2}{x_T^3}+2b\frac{x}{x_T^2}+c\frac{1}{x_T}\end{aligned}\tag{4}$$

where $\lambda_d(x)$ denotes desired LOS angle, $\lambda_d'(x)$ denotes the range derivative of desired LOS angle, a, b, c and d denotes coefficients.

Consider following boundary conditions at initial point

$$\begin{aligned}&\lambda_d(x_0)=\lambda_0=\arctan\left(\frac{y_T-y_0}{x_T-x_0}\right)\\&\lambda_d'(x_0)=\lambda_0'=-\frac{\sin(\gamma_0-\lambda_0)}{\cos\gamma_0\sqrt{(x_T-x_0)^2+(y_T-y_0)^2}}\end{aligned}\tag{5}$$

and following boundary conditions at endgame point

$$\lambda_d(x_T)=\gamma_d,\lambda_d'(x_T)=0\tag{6}$$

Substituting (5) and (6) into (4), one can obtain that

$$\begin{aligned}&a\frac{x_0^3}{x_T^3}+b\frac{x_0^2}{x_T^2}+c\frac{x_0}{x_T}+d=\lambda_0,\\&3a\frac{x_0^2}{x_T^3}+2b\frac{x_0}{x_T^2}+c\frac{1}{x_T}=\lambda_0',\\&3a\frac{1}{x}+2b\frac{1}{x}+c\frac{1}{x}=0,\\&a+b+c+d=\gamma_d\end{aligned}\tag{7}$$

Solving (7) yields

$$\begin{aligned}a&=-\frac{2x_T^3(\gamma_d-\lambda_0)}{(x_T-x_0)^3}+\frac{x_T^3}{(x_T-x_0)^2}\lambda_0',\\b&=\frac{3x_T^3(x_0+x_T)(\gamma_d-\lambda_0)}{(x_T-x_0)^3}-\frac{x_T^2(x_0+2x_T)}{(x_T-x_0)^2}\lambda_0',\\c&=-\frac{6x_0x_T^2(\gamma_d-\lambda_0)}{(x_T-x_0)^3}+\frac{x_T^2(2x_0+x_T)}{(x_T-x_0)^2}\lambda_0'\\d&=\frac{\gamma_dx_0^2(3x_T-x_0)+\lambda_0x_T^2(x_T-3x_0)}{(x_T-x_0)^3}-\frac{x_0x_T^2}{(x_T-x_0)^2}\lambda_0'\end{aligned}\tag{8}$$

2.3 Time-to-go estimation

The method for time-to-go estimation is the key point in the practice of impact time and angle constrained guidance. Ref. (Jeon et al., 2010)stated a kind of time-to-go prediction method as (9) for planar engagement case and Ref.(He and Lin, 2018) extended this method into three-dimensional

environment.

$$t_{go}=\frac{r}{V}\left(1+\frac{\sigma^2}{2(2N-1)}\right) \tag{9}$$

where N denotes navigation gain.

However, above time-to-go estimation method without terminal impact angle information only can be employed when the interceptor utilizes PN guidance law. To obtain time-to-go for other guidance laws, Ref.(kumar and Ghose, 2015) proposed a novel 2D time-to-go estimation algorithm using linear approximation technique, which is formulated as

$$t_{go}=\frac{r}{V}\left(1+\frac{\sigma^2+\sigma_f^2}{15}-\frac{\sigma\sigma_f}{30}-\frac{\sigma^4+\sigma_f^4}{420}+\frac{\sigma\sigma_f\left(\sigma^2+\sigma_f^2-\sigma\sigma_f\right)}{840}\right) \tag{10}$$

For ease of application, omitting fourth and fifth terms of (10), yields

$$t_{go}=\frac{r}{V}\left(1+\frac{\sigma^2+\sigma_f^2}{15}-\frac{\sigma\sigma_f}{30}\right) \tag{11}$$

where $\sigma_f=\gamma_d-\lambda$ denotes trajectory lead angle at endgame point.

Taking the derivative of (11) with respect to x yields

$$t'_{go}=\frac{r'}{V}\left(1+\frac{\sigma^2+\sigma_f^2}{15}-\frac{\sigma\sigma_f}{30}\right)+\frac{r}{V}\left(\frac{2\sigma\sigma'+2\sigma_f\sigma'_f}{15}-\frac{\sigma'\sigma_f+\sigma\sigma'_f}{30}\right) \tag{12}$$

It follows from the definitions of σ' and σ'_f that

$$\begin{aligned}\sigma'&=\gamma'-\lambda'=\frac{A}{V^2\cos\gamma}-\lambda'\\ \sigma'_f&=-\lambda'\end{aligned} \tag{13}$$

Substituting (13) into (12) yields

$$t'_{go}=\frac{r'}{V}\left(1+\frac{\sigma^2+\sigma_f^2}{15}-\frac{\sigma\sigma_f}{30}\right)+\frac{rA}{V^3\cos\gamma}\left(\frac{4\sigma-\sigma_f}{30}\right)-\frac{r\lambda'\left(\sigma+\sigma_f\right)}{10V} \tag{14}$$

For ease of following study, (14) is rewritten as follows

$$\begin{aligned}t'_{go}&=K_1+K_2A\\ K_1&=\frac{r'}{V}\left(1+\frac{\sigma+\sigma_f}{15}-\frac{\sigma\sigma_f}{30}\right)-\frac{r\lambda'\left(\sigma+\sigma_f\right)}{10V}\\ K_2&=\frac{r}{V^3\cos\gamma}\left(\frac{4\sigma-\sigma_f}{30}\right)\end{aligned} \tag{15}$$

2.4 Assumption and Lemma

Assumption 1. There exist two positive constants $r_{\max}$ and $r_{\min}$ such that $r_{\min}\le r\le r_{\max}$. The values of $r_{\max}$ and $r_{\min}$ are subject to the maximum distance between the missile and target and the length of missile's and target's shells, respectively.

Lemma 1. (Bhat and Bernstein, 2000) Assume that $V(x)$ is C^1 a smooth function defined on $U\in\mathbb{R}^n$. For arbitrary positive constants β_1 and $\beta_2\in(0,1)$, if there exists $\dot V(x)+\beta_1V^{\beta_2}(x)\le 0$, there exists an region $U_0\subset\mathbb{R}^n$ such that any $V(x)$ starting from this region can reach $V(x)\equiv 0$ in a finite time T_r, which is given by $T_r\le V^{1-\beta_2}(x_0)/\beta_1(1-\beta_2)$, where $V(x_0)$ is the initial value of $V(x)$.

3. GUIDANCE LAW DESIGN

Based on compound SMC theory, a super-twisting-like algorithm is employed to design guidance law for system (3), desired LOS angle (4), coefficients (8) and estimated time-to-go (11) in this section.

Select sliding manifold as

$$s=\eta\left(\lambda'-\lambda'_d\right)+(1-\eta)\left(t_{go}+t_{elap}-T_d\right) \tag{16}$$

where t_{elap} denotes elapsed time, T_d denotes desired impact time which is set up in advance, $\eta\in[0,1]$ is a constant meaning the weight.

Remark 2. Zeroing LOS angular rate methodology is not applicable in the case we take the derivatives of system variables with respect to x. At the initial point, real LOS angle $\lambda(x_0)$ is approximately equal to desired LOS angle $\lambda_d(x_0)$, thus, to guarantee the interceptor move following the desired trajectory, we only need to guarantee real LOS angular rate $\lambda'(x)$ converge to the desired LOS angle $\lambda'_d(x)$. Above guidance law design methodology does not only guarantee accurate interception, but guarantee impact heading angle constraint.

The robust guidance law is designed as

$$\begin{aligned}A&=A_{eq}+A_{dis}\\ A_{eq}&=\frac{(1-\eta)K_1rV^2\cos^3\gamma+(1-\eta)rV\cos^2\gamma+\eta rV^2\cos^3\gamma\left(\frac{2r'\lambda'}{r}+\frac{6ax}{x_T^3}+\frac{2b}{x_T^2}\right)}{\eta\cos\lambda+(1-\eta)K_2rV^2\cos^3\gamma}\\ A_{dis}&=\frac{\left(-k_1|s|^{(1-1/p)}\operatorname{sgn}(s)-k_2\varsigma\right)}{\operatorname{sgn}\left((1-\eta)K_2-\eta\cos\lambda/rV^2\cos^3\gamma\right)}\\ \varsigma'&=\frac{rV^2\cos^3\gamma}{\eta\cos\lambda+(1-\eta)K_2rV^2\cos^3\gamma}\cdot\frac{|s|^{(1-2/p)}\operatorname{sgn}(s)}{\operatorname{sgn}\left((1-\eta)K_2-\eta\cos\lambda/rV^2\cos^3\gamma\right)}\end{aligned} \tag{17}$$

where $k_1>0$, $k_2>0$ and $p>2$ are design parameters.

The closed-loop stability of system (3) with guidance law (17) can be summarized as following theorem.

Theorem 1. Guidance law (8) can drive system (3) converge into a small compact region around zero in a finite time.

Proof. Taking the derivative with respect to x, yields

$$\begin{aligned}s'&=\eta\left(\lambda''-\lambda''_d\right)+(1-\eta)\left(t'_{go}+t'_{elap}\right)\\ &=\eta\left(-\frac{\cos\lambda}{rV^2\cos^3\gamma}A-\frac{2r'\lambda'}{r}-\frac{6ax}{x_T^3}-\frac{2b}{x_T^2}\right)\\ &\quad+(1-\eta)\left(K_1+K_2A+\frac{1}{V\cos\gamma}\right)\end{aligned} \tag{18}$$

Substituting (17) into (18), yields

$$\begin{aligned}s'=&-k_1\kappa\frac{|s|^{(1-1/p)}\operatorname{sgn}(s)}{\operatorname{sgn}\left((1-\eta)K_2-\eta\cos\lambda/rV^2\cos^3\gamma\right)}\\ &-k_2\kappa\int\kappa\frac{|s|^{(1-2/p)}\operatorname{sgn}(s)}{\operatorname{sgn}\left((1-\eta)K_2-\eta\cos\lambda/rV^2\cos^3\gamma\right)}dx\end{aligned} \tag{19}$$

where

$$\kappa=\frac{rV^2\cos^3\gamma}{\eta\cos\lambda+(1-\eta)K_2rV^2\cos^3\gamma} \tag{20}$$

For ease of study, introduce following two auxiliary variables

$$\begin{aligned}\omega_1&=s\\ \omega_2&=-k_2\int\kappa\cdot\frac{|s|^{(1-2/p)}\operatorname{sgn}(s)}{\operatorname{sgn}\left((1-\eta)K_2-\eta\cos\lambda/rV^2\cos^3\gamma\right)}dx\end{aligned} \tag{21}$$

Next, following discuss is divided into two cases, with respect to the property of positive and negative of the

polynomial $(1-\eta)K_2-\eta\cos\lambda/rV^2\cos^3\gamma$.

Case 1: If $(1-\eta)K_2-\eta\cos\lambda/rV^2\cos^3\gamma>0$, (19) can be rewritten as

$$s'=-k_1\kappa|s|^{(1-1/p)}\operatorname{sgn}(s)-k_2\kappa\int\kappa|s|^{(1-2/p)}\operatorname{sgn}(s)dx \tag{22}$$

and (21) can be rewritten as

$$\begin{aligned}\omega_1&=s\\ \omega_2&=-k_2\int\kappa|s|^{(1-2/p)}\operatorname{sgn}(s)dx\end{aligned} \tag{23}$$

Differentiating (23) with respect to x, yields

$$\begin{aligned}\omega_1'&=-k_1\kappa|\omega_1|^{(1-1/p)}\operatorname{sgn}(\omega_1)+\kappa\omega_2\\ \omega_2'&=-k_2\kappa|\omega_1|^{(1-2/p)}\operatorname{sgn}(\omega_1)\end{aligned} \tag{24}$$

To demonstrate the finite-time convergent property, consider following Lyapunov function candidate

$$V=\frac{k_2p}{p-1}|\omega_1|^{2(p-1)/p}+\frac{1}{2}\omega_2^2+\frac{1}{2}\left(k_1|\omega_1|^{(p-1)/p}\operatorname{sgn}(\omega_1)-\omega_2\right)^2 \tag{25}$$

It follows from (25) that $V\ge0$ at any time, so that V can be employed to evaluate the closed-loop stability.

Differentiating (25) with respect to x, yields

$$\begin{aligned}V'=&\left(\frac{k_2p}{p-1}+\frac{1}{2}k_1^2\right)\frac{2p-2}{p}|\omega_1|^{(p-2)/p}\operatorname{sgn}(\omega_1)\dot\omega_1+2\omega_2\dot\omega_2\\ &-k_1|\omega_1|^{(p-1)/p}\operatorname{sgn}(\omega_1)\dot\omega_2-k_1\frac{p-1}{p}|\omega_1|^{-1/p}\omega_2\dot\omega_1\\ =&\left(\frac{k_2p}{p-1}+\frac{1}{2}k_1^2\right)\frac{2p-2}{p}|\omega_1|^{(p-2)/p}\operatorname{sgn}(\omega_1)\left(\kappa\omega_2-k_1\kappa|\omega_1|^{(p-1)/p}\operatorname{sgn}(\omega_1)\right)\\ &+\left(2\omega_2-k_1|\omega_1|^{(p-1)/p}\operatorname{sgn}(\omega_1)\right)\left(-k_2\kappa|\omega_1|^{(p-2)/p}\operatorname{sgn}(\omega_1)\right)\\ &-k_1\frac{p-1}{p}|\omega_1|^{-1/p}\omega_2\left(\kappa\omega_2-k_1\kappa|\omega_1|^{(p-1)/p}\operatorname{sgn}(\omega_1)\right)\\ =&-\kappa|\omega_1|^{-1/p}\left(k_1k_2|\omega_1|^{2(p-1)/p}+\frac{p-1}{p}k_1^3|\omega_1|^{2(p-1)/p}\right)\\ &-\kappa|\omega_1|^{-1/p}\left(-\frac{2p-2}{p}k_1^2|\omega_1|^{(p-1)/p}\operatorname{sgn}(\omega_1)\omega_2+\frac{p-1}{p}k_1\omega_2^2\right)\end{aligned} \tag{26}$$

It follows from $(1-\eta)K_2-\eta\cos\lambda/rV^2\cos^3\gamma>0$ and Assumption 1 that $\kappa>0$, and there exist $\kappa_{\min}>0$ and $\kappa_{\max}>0$ such that

$$\kappa_{\min}\le\kappa\big|_{\kappa\in\mathbb{R}}\le\kappa_{\max} \tag{27}$$

Choosing $\boldsymbol{\omega}=\left[|\omega_1|^{(p-1)/p}\operatorname{sgn}(\omega_1),\omega_2\right]^T$, (26) can be rewritten as

$$V'=-\kappa|\omega_1|^{-1/p}\boldsymbol{\omega}^T\boldsymbol{Q}\boldsymbol{\omega}\le-\kappa_{\min}|\omega_1|^{-1/p}\boldsymbol{\omega}^T\boldsymbol{Q}\boldsymbol{\omega} \tag{28}$$

with

$$\boldsymbol{Q}=\begin{bmatrix}k_1k_2+k_1^3\dfrac{p-1}{p} & -k_1^2\dfrac{p-1}{p}\\ -k_1^2\dfrac{p-1}{p} & k_1\dfrac{p-1}{p}\end{bmatrix} \tag{29}$$

It follows from the definition of k_1, k_2 and p that $\boldsymbol{Q}$ is positive definite.

Next, rewrite (27) as

$$V=\boldsymbol{\omega}^T\boldsymbol{P}\boldsymbol{\omega} \tag{30}$$

with

$$\boldsymbol{P}=\frac{1}{2}\begin{bmatrix}\dfrac{k_2p}{p-1}+k_1^2 & -k_1\\ -k_1 & 2\end{bmatrix} \tag{31}$$

According to the definition of k_1, k_2 and p, one can conclude that $\boldsymbol{P}$ is positive definite and V is Radial unbounded, so that

$$\lambda_{\min}(\boldsymbol{P})\|\boldsymbol{\omega}\|^2\le V\le\lambda_{\max}(\boldsymbol{P})\|\boldsymbol{\omega}\|^2 \tag{32}$$

where $\lambda_{\min}(\cdot)$ and $\lambda_{\max}(\cdot)$ denote the minimum and maximum eigenvalues of $(\cdot)$.

It follows from $\|\boldsymbol{\omega}\|=\sqrt{|\omega_1|^{2(p-1)/p}+\omega_2^2}\ge|\omega_1|^{(p-1)/p}$ that $|\omega_1|^{-1/p}\ge\|\boldsymbol{\omega}\|^{-1/(p-1)}$, combining with (28) and (32), one can imply that

$$\begin{aligned}V'&\le-\|\boldsymbol{\omega}\|^{-1/(p-1)}\kappa_{\min}\lambda_{\min}(\boldsymbol{Q})\|\boldsymbol{\omega}\|^2\\ &\le-\lambda_{\min}(\boldsymbol{Q})\kappa_{\min}\|\boldsymbol{\omega}\|^{(2p-3)/(p-1)}\\ &\le-\frac{\kappa_{\min}\lambda_{\min}(\boldsymbol{Q})}{\lambda_{\max}(\boldsymbol{P})^{(2p-3)/(p-1)}}V^{(2p-3)/(p-1)}\end{aligned} \tag{33}$$

It follows from $p>2$ that $(2p-3)/(p-1)\in(0,0.5)$, according to Lemma 1, one can conclude the system will converge to a small neighbourhood around zero in a finite time, which is govern by

$$T_{reach}\le\frac{V_0^{1-(2p-3)/(p-1)}}{\dfrac{\kappa_{\min}\lambda_{\min}(\boldsymbol{Q})}{\lambda_{\max}(\boldsymbol{P})^{(2p-3)/(p-1)}}\left(1-(2p-3)/(p-1)\right)} \tag{34}$$

Case 2: If $(1-\eta)K_2-\eta\cos\lambda/rV^2\cos^3\gamma<0$, (19) can be rewritten as

$$s'=k_1\kappa|s|^{(1-1/p)}\operatorname{sgn}(s)+k_2\kappa\int\kappa|s|^{(1-2/p)}\operatorname{sgn}(s)dx \tag{35}$$

and (21) can be rewritten as

$$\begin{aligned}\omega_1&=s\\ \omega_2&=k_2\int\kappa|s|^{(1-2/p)}\operatorname{sgn}(s)dx\end{aligned} \tag{36}$$

Differentiating (34) with respect to x, yields

$$\begin{aligned}\omega_1'&=k_1\kappa|\omega_1|^{(1-1/p)}\operatorname{sgn}(\omega_1)+\kappa\omega_2\\ \omega_2'&=k_2\kappa|\omega_1|^{(1-2/p)}\operatorname{sgn}(\omega_1)\end{aligned} \tag{37}$$

Consider another Lyapunov function candidate

$$V=\frac{k_2p}{p-1}|\omega_1|^{2(p-1)/p}+\frac{1}{2}\omega_2^2+\frac{1}{2}\left(k_1|\omega_1|^{(p-1)/p}\operatorname{sgn}(\omega_1)+\omega_2\right)^2 \tag{38}$$

Differentiating (36) yields

$$\begin{aligned}V'=&\left(\frac{k_2p}{p-1}+\frac{1}{2}k_1^2\right)\frac{2p-2}{p}|\omega_1|^{(p-2)/p}\operatorname{sgn}(\omega_1)\omega_1'+2\omega_2\omega_2'\\ &+k_1|\omega_1|^{(p-1)/p}\operatorname{sgn}(\omega_1)\omega_2'+k_1\frac{p-1}{p}|\omega_1|^{-1/p}\omega_2\omega_1'\\ =&\left(\frac{k_2p}{p-1}+\frac{1}{2}k_1^2\right)\frac{2p-2}{p}|\omega_1|^{(p-2)/p}\operatorname{sgn}(\omega_1)\left(\kappa\omega_2+k_1\kappa|\omega_1|^{(p-1)/p}\operatorname{sgn}(\omega_1)\right)\\ &+\left(2\omega_2+k_1|\omega_1|^{(p-1)/p}\operatorname{sgn}(\omega_1)\right)k_2\kappa|\omega_1|^{(p-2)/p}\operatorname{sgn}(\omega_1)\\ &+k_1\frac{p-1}{p}|\omega_1|^{-1/p}\omega_2\left(\kappa\omega_2+k_1\kappa|\omega_1|^{(p-1)/p}\operatorname{sgn}(\omega_1)\right)\\ =&\kappa|\omega_1|^{-1/p}\left(k_1k_2|\omega_1|^{2(p-1)/p}+\frac{p-1}{p}k_1^3|\omega_1|^{2(p-1)/p}\right)\\ &+\kappa|\omega_1|^{-1/p}\left(\frac{2p-2}{p}k_1^2|\omega_1|^{(p-1)/p}\operatorname{sgn}(\omega_1)\omega_2+\frac{p-1}{p}k_1\omega_2^2\right)\end{aligned} \tag{39}$$

It follows from $(1-\eta)K_2-\eta\cos\lambda/rV^2\cos^3\gamma<0$ and Assumption 1 that $\kappa<0$, and there exist $\kappa_{\min}<0$ and $\kappa_{\max}<0$ such that

$$\kappa_{\min}\le\kappa\big|_{\kappa\in\mathbb{R}}\le\kappa_{\max} \tag{40}$$

Following part of demonstration is similar as Case 1. This completes the proof.

Remark 3. It follows from (17) that the polynomial

$(1-\eta)K_2 - \eta\cos\lambda/rV^2\cos^3\gamma$ serves as denominator and cannot be zero. However, in real engineering practice, the case $(1-\eta)K_2 - \eta\cos\lambda/rV^2\cos^3\gamma = 0$ may exist and cause guidance law (17) failure. To overcome this problem, we define that this polynomial should be a small value when it approximates zero.

4. SIMULATION EXAMPLES

In order to demonstrate the effectiveness of proposed guidance law, numerical simulations are carried out and the results are given and analysed in this section. The simulation is divided into three scenarios.

Scenario 1. Different desired flight times with the same impact angle.

We set up different desired flight times before simulation, in the presence of the same impact angle. During the homing phase, the guidance factors are chosen as Table.1.

Table.1 The guidance factors

Initial position	(0m, -500m)
Desired position	(10000m, 0m)
Desired flight times	45s, 50s, 54s
Velocity	250m/s
Initial heading angle	60°
Desired impact heading angle	-60°

The parameters as chosen as $k_1 = 50$, $k_2 = 10$ and $p = 2.5$.

Simulation results are shown as Fig.2

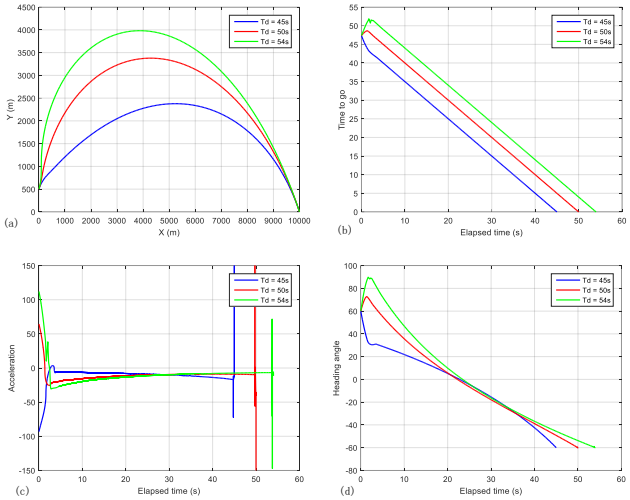

Fig.2 Simulation results of Scenario 1: (a) Trajectories; (b)Time-to-go; (c) Accelerations; (d) Heading angles.

It follows from Fig.2(a) that the missile can intercept the target accurately with a same heading angle. Note that the trajectory is longer when the desired time is longer. Fig.2(b) depicts the time-to-go and it can be concluded that missile arrives to target point at the desired time accurately. Figs.2(c) and (d) depict the acceleration and heading angle, one can see that heading angle approaches to the desired value at terminal point.

Scenario 2. Different desired heading angles with the same flight time.

We set up different desired heading angles in advance in the presence of the same flight time. The guidance factors are chosen as Table.2.

Table.2 The guidance factors

Initial position	(0m, -500m)
Desired position	(10000m, 0m)
Desired flight time	45s
Velocity	250m/s
Initial heading angle	60°
Desired heading angles	0°, -30°, -45°, -60°, -90°

The parameters are selected same as them in Scenario 1.

Simulation results are shown as Fig.3.

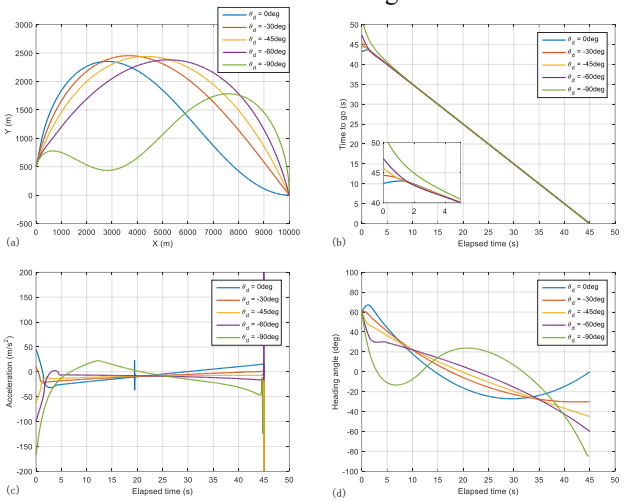

Fig.3 Simulation results of Scenario 2: (a) Trajectories; (b)Time-to-go; (c) Accelerations; (d) Heading angles.

Figs.3(a), (b), (c) and (d) depict trajectory, time-to-go, acceleration and heading angles, respectively. From Figs.3(b) and (d), one can see that the missile can intercept target with desired impact angles and a same flight time.

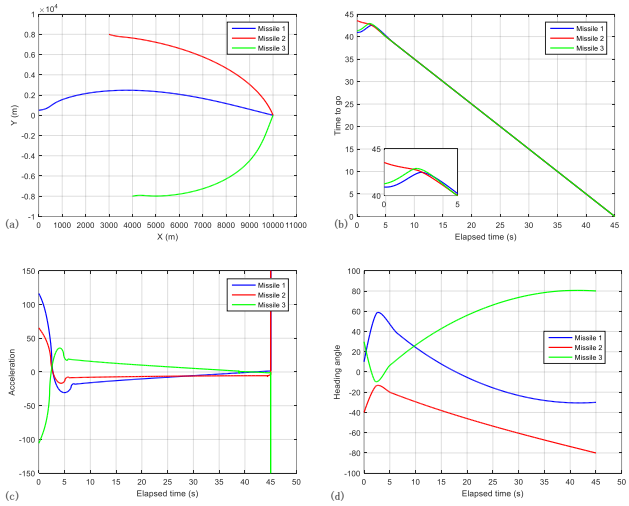

Fig.4 Simulation results of Scenario 3: (a) Trajectories; (b)Time-to-go; (c) Accelerations; (d) Heading angles.

Scenario 3. Multiple missiles salvo-attack.

In this scenario, we employ three missiles to achieve the

mission of salvo-attack. These missiles launch from different position at different initial heading angles, but intercept the target simultaneously with desired heading angles. The guidance factors of every missile are set up as Table.3.

Table.3. The guidance factors

	Missile 1	Missile 2	Missile 3
Initial position	(0,500)	(3000,8000)	(4000,-8000)
Initial angle	10º	-40º	30º
Desired angle	-30º	80º	-80º
Desired time	45s	45s	45s

The parameters are selected same as them in Scenario 1. Simulation results are shown as Fig.4.

Fig.4(a) illustrates trajectories of three missiles and these missile approach to target point accurately. Fig.4(b) shows that all the missiles hold a same flight time. Fig.4(c) depicts accelerations of every missile. As shown as Fig.4(d), one can see that every missile can achieve desired impact angle at the terminal time.

5. CONCLUSION

Facing salvo-attack missions, a guidance law which can achieve accurate interception and impact time and angle constraints is proposed in this paper. This guidance law only uses four parameter and is practical. Simulation examples verify its efficiency and effectiveness properties.

REFERENCES

BARDHAN, R. & GHOSE, D. 2015. Nonlinear Differential Games-Based Impact-Angle-Constrained Guidance Law. *Journal of Guidance, Control, and Dynamics,* 38**,** 384-402.

BHAT, S. P. & BERNSTEIN, D. S. 2000. Finite-Time Stability of Continuous Autonomous Systems. *SIAM Journal on Control and Optimization,* 38**,** 751-766.

CHO, D., KIM, H. J. & TAHK, M.-J. 2015. Nonsingular Sliding Mode Guidance for Impact Time Control. *Journal of Guidance, Control, and Dynamics,* 39**,** 61-68.

FRANZINI, G., TARDIOLI, L., POLLINI, L. & INNOCENTI, M. 2017. Visibility Augmented Proportional Navigation Guidance. *Journal of Guidance, Control, and Dynamics,* 41**,** 987-995.

HE, S. & LIN, D. 2018. Three-Dimensional Optimal Impact Time Guidance for Antiship Missiles. *Journal of Guidance, Control, and Dynamics,* 42**,** 941-948.

HOU, Z., YANG, Y., LIU, L. & WANG, Y. 2019. Terminal sliding mode control based impact time and angle constrained guidance. *Aerospace Science and Technology,* 93**,** 105142.

JEON, I.-S., LEE, J.-I. & TAHK, M.-J. 2010. Homing Guidance Law for Cooperative Attack of Multiple Missiles. *Journal of Guidance, Control, and Dynamics,* 33**,** 275-280.

JI, Y., LIN, D., WANG, W., HU, S. & PEI, P. 2019. Three-dimensional terminal angle constrained robust guidance law with autopilot lag consideration. *Aerospace Science and Technology,* 86**,** 160-176.

KUMAR, S. R. & GHOSE, D. 2015. Impact Time and Angle Control Guidance. *AIAA Guidance, Navigation, and Control Conference.* American Institute of Aeronautics and Astronautics.

KUMAR, S. R., RAO, S. & GHOSE, D. 2014. Nonsingular Terminal Sliding Mode Guidance with Impact Angle Constraints. *Journal of Guidance, Control, and Dynamics,* 37**,** 1114-1130.

LYU, T., GUO, Y., LI, C., MA, G. & ZHANG, H. 2019a. Multiple missiles cooperative guidance with simultaneous attack requirement under directed topologies. *Aerospace Science and Technology,* 89**,** 100-110.

LYU, T., LI, C., GUO, Y. & MA, G. 2019b. Three-dimensional finite-time cooperative guidance for multiple missiles without radial velocity measurements. *Chinese Journal of Aeronautics,* 32**,** 1294-1304.

SUN, L., WANG, W., YI, R. & XIONG, S. 2016. A novel guidance law using fast terminal sliding mode control with impact angle constraints. *ISA Transactions,* 64**,** 12-23.

TALOLE, S. E., GHOSH, A. & PHADKE, S. B. 2006. Proportional navigation guidance using predictive and time delay control. *Control Engineering Practice,* 14**,** 1445-1453.

TSALIK, R. & SHIMA, T. 2016. Optimal Guidance Around Circular Trajectories for Impact-Angle Interception. *Journal of Guidance, Control, and Dynamics,* 39**,** 1278-1291.

WANG, X. H. & TAN, C. P. 2018. 3-D impact angle constrained distributed cooperative guidance for maneuvering targets without angular-rate measurements. *Control Engineering Practice,* 78**,** 142-159.

YANG, Z., WANG, H., LIN, D. & ZANG, L. 2016. A New Impact Time and Angle Control Guidance Law for Stationary and Nonmaneuvering Targets %J International Journal of Aerospace Engineering. 2016**,** 14.

ZARCHAN, P. 1995. Proportional navigation and weaving targets. *Journal of Guidance, Control, and Dynamics,* 18**,** 969-974.

ZHAO, Y., SHENG, Y. & LIU, X. 2016. Analytical impact time and angle guidance via time-varying sliding mode technique. *ISA Transactions,* 62**,** 164-176.

ZHU, J., SU, D., XIE, Y. & SUN, H. 2019. Impact time and angle control guidance independent of time-to-go prediction. *Aerospace Science and Technology,* 86**,** 818-825.